Finite Elements in Analysis and Design ▮ (▮▮▮▮) ▮▮▮–▮▮▮

Contents lists available at ScienceDirect

Finite Elements in Analysis and Design

journal homepage: www.elsevier.com/locate/finel

On a new 3D primal-mixed finite element approach for thermal stress analysis of multi-layered geometrically multiscale structures

Dubravka Mijuca *

Faculty of Civil Construction Management, University UNION, Cara Dusana 62–64, 11000 Belgrade, Serbia

ARTICLE INFO

Article history:
Received 12 December 2008
Received in revised form
20 October 2009
Accepted 23 November 2009

Keywords:
Primal-mixed finite element
Multiscale reliability
Scale resolution
Material interface
Inf-sup test
Thermal stress
Heterogeneous materials

ABSTRACT

This paper presents a new reliable fully three-dimensional time efficient primal-mixed finite element approach with continuous *primal* and dual variables in geometrically *multiscale* thermoelasticity. The semi-coupling between thermal and mechanical physical fields is achieved straightforwardly via essential boundary condition per stress, and without *consistency* error. The direct sparse solver and matrix scaling routine are used for the solution of resulting large scale indefinite systems of linear equations. It will be shown that present solid finite element HC8/27 passes the first and the second stability condition (inf-sup test) for highly distorted finite elements with aspect ratio up to 7 orders of magnitude, for both, compressible and nearly incompressible materials. A number of pathological benchmark model problems, with material interfaces or coatings, with geometrical scale resolutions up to 8 orders of magnitude and aspect ratio of finite elements up to 7 orders of magnitude, are examined to test the robustness and execution times. It is shown that by rapid varying of spatial scale over local heterogeneities, the singularity of stress is captured without oscillation. It is shown that, if needed, present approach can simulate the simplified theories, as *beam* and *plate* theories, if the same restrictions on the stress tensor components are imposed. The new definition of multiscale reliability is given.

1. Introduction

The growing interest in the multiscale analysis of structures with complex micro-structural geometry and behavior, can be observed. Consequently, the primary goal of the manuscript is to present a systematic approach in semi-coupled thermo-mechanical analysis at multiple spatial scales.

The new straightforward, reliable, coordinate independent and time-efficient *primal-mixed* finite element numerical simulation procedure for the geometrically multiscale heterogeneous solid body model problems in unconditionally stable and consistent transient thermo-mechanical analysis, where both, *primal* and *dual* variables can be imposed as essential boundary condition, is presented.

The other state of the art procedures in coupling of various physical processes over the temporal and spatial scales are recently introduced, also. For example, a multiscale space–time asymptotic homogenization procedure for analyzing multiple physical processes interacting at multiple spatial and temporal scales is developed and applied to the coupled thermo-viscoelastic composites, is presented in [1]. It was shown that by rapidly varying spatial and temporal scales, the oscillations induced by local heterogeneities at diverse time scales, can be captured. Further, two-scale thermo-mechanical analysis framework for heterogeneous solids based on a computational homogenization technique where thermo-mechanical approaches at both scales are treated consistently and linked by a rigorous scale bridging procedure, in a nested finite element solution procedure with an operator-split implementation, is presented in [2].

In addition, different finite element approaches are abundantly used in structural mechanics in the past several decades. Nevertheless, when it is based on standard, one field, so-called *primal* finite element approach it cannot be straightforwardly used in analyses over the multiple spatial scales. Specifically, this approaches are not stable [3] when finite elements are extremely distorted, thin or nearly incompressible, where there are spurious oscillations of stresses due to the volumetric locking. In addition, if it is based on dimensional reduction [4] it suffers from hourglass locking [5,6].

More, stress equilibrium is violated inside each finite element because the stress is calculated *a posteriori*. Therefore, stresses are discontinuous across elements, stresses are not in equilibrium with the applied traction and there is not possibility to apply stresses as essential boundary conditions. Further, in coupled problems, as thermal and mechanical, we can have consistency error [7] between resulting thermal and mechanical stresses. These problems are only greater in multiscale analysis, due to the

* Tel.: +381 11 2180 287; fax: +381 11 2180 013.
E-mail addresses: dmijuca@fgm.edu.yu, dmijuca@sezampro.rs.

0168-874X/$ - see front matter © 2009 Elsevier B.V. All rights reserved.
doi:10.1016/j.finel.2009.11.001

high scale resolution of significant digits in calculations. It is recognized that mixed finite element approach, which have all variables of interest as solution variables (and not just a one per physical problem of interest) are less sensitive in the above-mentioned pathological situations [8,9].

Nevertheless, mixed finite elements did not yet find wide acceptance in *solid* mechanics, although it is proved in [10,11] that primal-mixed finite element approach where all variables of interest are continuous, is reliable. It was primarily due to the misleading opinion that it requires much more execution time to be solved because of the larger system matrix than in corresponding *primal* approach. In addition, some authors [9] comment: "…The use of C^0 discretization for the stress field should be avoided. The main reason for this is the difficulty in the numerical solution of the linear system of equations…". Nevertheless, it was shown [10,11] that it is possible to develop reliable primal-mixed finite elements having C^0 discretization for the dual variables (e.g. heat flux, stress), also. In addition, the present finite element approach in combination with this sparse solver MA57 [12] and matrix scaling routine MC64 [17], is efficient in time and storage [13]. It is shown that it is at least two orders of magnitude faster than previously used in-house solver based on simple Gaussian elimination.

In the present paper we will show that unconditionally stable transient heat transfer HCT/q [11] and mechanical HCu/t [10] reliable primal-mixed finite element approaches, could be straightforwardly semi-coupled via essential boundary condition per stress variable in order to solve multiscale thermo mechanical problems in multimaterial solid mechanics.

It will be shown that present finite element HC8/27 passes second stability condition (inf-sup test) for aspect ratio up to 7 orders of magnitude, for regular or highly distorted finite element meshes, in compressible and nearly incompressible materials. That makes the present finite element suitable with bridging the scales with simulation approaches on particle levels [14].

The essential contribution of the present research is that it enables fast and reliable solution of fully three-dimensional transient thermo-mechanical response of *geometrically multiscale* multimaterial model problems, using small number of finite elements for the complexity of the model problem.

We will use the next terminology in the present text. Geometrical *scale resolution* stands for the ratio between maximal axial dimension of the model problem and minimal axial dimension of finite elements, while *aspect ratio* stands for the ratio between maximal and minimal axial dimension of a finite element.

In addition, the new definition should be stated: *Some numerical approximation procedure is multiscale reliable if it is reliable throughout all geometrical scale in which underlying physical law is valid.*

The behavior of the proposed primal-mixed approach, where all variables of interest are taken to be continuous, will be examined on the number of numerical examples in transient thermo-mechanics multi-phased materials with material discontinuities. Primarily, it will be tested if present approach is capable to mimic the analytical solution obtained by dimensional reduction theories, as beam, plate and shell theories, and how the target solution is changed if there is no simplification of geometry or stress tensor. Consequently, it will be shown that there is inconsistency in results obtained by classical *beam* and *plate* theories and present full theory approach, which can be motive for the further experimental measurements. It can explain reasons for premature collapse in building under fire, far before design solutions obtained by dimensional reduction theories. Nevertheless, it is presently confirmed that dimensional reduction and neglecting of some stress components leads to substantial underestimation of maximal thermal stresses.

Consequently, new target values for beam and plate-like model problems obtained by the present approach without simplifications will be proposed. More, it will be tested how results are changed if the finite element mesh is substantially degenerated.

In addition, it will be shown that by using one to several micron thin layers of finite elements left and right of material discontinuities, robustness and accuracy of the procedure is retained, regardless of the local violation of discontinuity of the some of the stress components on the material interface. In addition, the use of the continuous functions for approximation of all stress components enables natural continuity of stress field over discontinuity-free regions of the body, which is not possible in standard displacement-based finite element methods in which *a posteriori* stress recovery methods should be utilized.

2. Field problems

We will start from the special primal-mixed weak form in transient heat transfer [11]:

Find $\{T, \boldsymbol{q}\} \in H^1 \times H^{1n}$ such that $T|_{\partial\Omega_T} = \overline{T}$ and

$$\int_\Omega \boldsymbol{q}\boldsymbol{k}^{-1}\mathbf{Q}\,d\Omega + \int_\Omega \nabla T \cdot \mathbf{Q}\,d\Omega = \int_\Omega \rho c \frac{\partial T}{\partial t}\theta\,d\Omega + \int_\Omega \boldsymbol{q} \cdot \nabla\theta\,d\Omega - \int_\Omega \theta f\,d\Omega - \int_{\partial\Omega_q} \theta q_h\,d\partial\Omega - \int_{\partial\Omega_c} q_c\theta\,d\partial\Omega \tag{1}$$

for all $\{\theta, \mathbf{Q}\} \in H^1 \times H^{1n}$. such that $\theta|_{\partial\Omega_T} = 0$.

As an essential contribution of the present approach, the trial and test shape functions for the heat flux variable are presently chosen from continuous subspace H^1, instead from subspace L_2.

The Backward Euler scheme is used for the time discretization, where:

$$\rho c \frac{\partial T}{\partial t}\bigg|_n \approx \rho c \frac{{}^nT - {}^{n-1}T}{\Delta t} \tag{2}$$

For solving the behavior of the solid body under mechanical loading, Hellinger–Reissner's principle [10] is used:

Find $\{\boldsymbol{u}, \boldsymbol{t}\} \in H^{1n} \times H^{1n\times n}_{sym}$ such that $\boldsymbol{u}|_{\partial\Omega_t} = \boldsymbol{w}$ and

$$\int_\Omega (\boldsymbol{A}\boldsymbol{t} : \boldsymbol{s} - \boldsymbol{s} : \nabla\boldsymbol{u} - \nabla\boldsymbol{v} : \boldsymbol{t})\,d\Omega = -\int_\Omega \boldsymbol{v}\cdot\boldsymbol{f}\,d\Omega - \int_{\partial\Omega_t} \boldsymbol{v}\cdot\boldsymbol{p}\,d\partial\Omega. \tag{3}$$

for all $\{\boldsymbol{v}, \boldsymbol{s}\} \in H^{1n} \times H^{1n\times n}_{sym}$ such that $\boldsymbol{v}|_{\partial\Omega_t} = 0$.

It should be noted that in the original version of Hellinger–Reissner's principle [3,8] stresses are chosen from discontinuous subspaces $L^{2n\times n}_{\text{sym}}$.

In above expressions T, $\boldsymbol{q}$, $\boldsymbol{u}$ and $\boldsymbol{t}$ are the temperature, heat flux, displacement and stress trial variables, respectively, while, θ, $\mathbf{Q}$, $\boldsymbol{v}$ and $\boldsymbol{s}$ are their test variables, respectively. The quantity $\boldsymbol{k}$ is a second order tensor of thermal conductivity. If the material is homogeneous and isotropic, the tensor $\boldsymbol{k}$ will degenerate to simple scalar value k, i.e. thermal conductivity. Further, ρ is the material density, and c the specific heat, while f stands for the internal heat source generated per unit volume.

The $\boldsymbol{A}$ is the fourth order compliance matrix tensor. The $\boldsymbol{f}$ is the body force, and the $\boldsymbol{p}$ is the vector of the prescribed boundary tractions. $H^{1n\times n}_{\text{sym}}$ is the space of all symmetric tensorfields that are square integrable and have square integrable gradients, while H^{1n} is the space of all vectors that are square integrable and have square integrable gradients.

The displacements and stresses are chosen from continuous subspaces, which is correct for discontinuity-free regions of solid body. Nevertheless, on the surfaces of material discontinuities all components of stresses are discontinuous except transversal stress component. Violation of the discontinuity will be presently

Please cite this article as: D. Mijuca, On a new 3D primal-mixed finite element approach for thermal stress analysis of multi-layered geometrically multiscale structures, Finite Elem. Anal. Des. (2009), doi:10.1016/j.finel.2009.11.001

prevailed by placing micron thin layer of finite elements adjacent to discontinuity surface.

It will be shown that essential contribution of the present investigation is that calculated temperatures are introduced directly in field Eq. (3), that is, without differentiation. It will be done through essential boundary conditions per stresses. We can see from (1) and (3) that temperatures and stresses are presently approximated by the functions of the same polynomial degree. In addition, constitutive equation between stress and thermal strain presently does not include derivative of temperature. Therefore, there will be no *consistency error* between calculated thermal and stress deformation fields [15].

It should be noted that *consistency error* is a big shortcoming of primal finite element approaches. In primal approaches polynomial degree of thermal strains is lower than polynomial degree of mechanical strains, if temperatures and displacements are approximated by the functions of the same polynomial degree.

2.1. Introduction of prescribed thermal strains

In the case of traditional materials where there is no heat production due to strain rate, thermal effects on a body are limited to strains due to the temperature gradient, which are autonomously determined and constitute only a datum for stress analysis [16]. Therefore, strains are mechanical ($\boldsymbol{e}_p^M$) or thermal ($\boldsymbol{e}_p^T$), and additive in the linear case.

In *primal* finite element approaches, temperature enters mechanical field equations (**Ku=F**) through force loading term **f**, by differentiation of the thermal strains. Consequently, thermal strains will be in one degree lower polynomial function space that mechanical strains. That leads to the *consistency error* between mechanical and thermal stresses [7,14], and spurious oscillations of results, especially in the vicinity of singularity or high gradient of heat flux. It can be avoided only if polynomial degree of approximation function of displacement is one order higher than for temperature.

On the other hand, in the present approach thermal strain enters the mechanical formulation (3) as essential boundary condition per stress, using constitutive equation. To be precise, the corresponding prescribed thermal strains $\boldsymbol{e}_T^p$ are calculated from prescribed temperatures T_p using next constitutive equation:

$$\boldsymbol{e}_T^p = \alpha(T_p - T) \tag{4}$$

where α is second order tensor of thermal expansion coefficients (scalar in the case of isotropic materials), while T_i is the initial temperature. The prescribed thermal stresses $\boldsymbol{t}_T^p$ are then simply calculated from strains $\boldsymbol{e}_p^T$ via constitutive relation:

$$\boldsymbol{t}_T^p = C : \boldsymbol{e}_T^p \tag{5}$$

where $\boldsymbol{C}$ is the elasticity matrix.

We can see from (1) and (3) that presently thermal stresses and mechanical stresses are calculated in the subspaces of the interpolation functions of the same degree without any loss in accuracy. Therefore, we can say that semi-coupling of thermal and mechanical physical problem is presently performed in the consistent way.

2.2. Finite element equations

The present primal-mixed finite-element approaches in elastostatics (HCu/t), and in transient heat (HCT/q), were introduced in [10] and [11], respectively. It is proved that these procedures are reliable [3,5], and thus not sensitive to locking [6,8].

The finite-element equation of the present transient heat approach is given by [11]

$$\begin{bmatrix} A_{vv} & B_{vv}^T \\ B_{vv} & -U_{vv}-S_{vv} \end{bmatrix} \begin{bmatrix} \mathbf{q}_v \\ T_v \end{bmatrix} = \begin{bmatrix} -A_{vp} & -B_{vp}^T \\ -B_{vp} & U_{vp} \end{bmatrix} \begin{bmatrix} \mathbf{q}_p \\ T_p \end{bmatrix} + \begin{bmatrix} 0 & 0 \\ 0 & S_{vp} \end{bmatrix} \begin{bmatrix} 0 \\ T_p^{(t-1)} \end{bmatrix} + \begin{bmatrix} 0 \\ F_p + H_p - K_p \end{bmatrix} + \begin{bmatrix} 0 \\ -L_p^{(t-1)} \end{bmatrix} \tag{6}$$

where

$$\begin{aligned} A_{\Lambda p \Gamma r} &= \sum_e \int_{\Omega_e} \Omega_\Lambda^L g_{(L)p}^a V_L k_{ab}^{-1} g_{(M)r}^b V_M \Omega_\Gamma^M \, d\Omega_e; \\ B_{\Lambda p \Gamma} &= \sum_e \int_{\Omega_e} \Omega_\Lambda^L g_{(L)p}^a V_L P_{M,a} \Omega_\Gamma^M \, d\Omega_e \\ U_{\Lambda\Gamma} &= \sum_e \int_{\partial\Omega_{ce}} h_c \Omega_\Lambda^L P_L P_M \Omega_\Gamma^M \partial\Omega_{ce}; \\ F_\Gamma &= \sum_e \int_{\Omega_e} \Omega_\Gamma^M P_M s \, d\Omega_e S_{\Lambda\Gamma} = \sum_e \int_{\Omega_e} \frac{\rho c}{\Delta t} \Omega_\Lambda^L P_L P_M \Omega_\Gamma^M \, d\Omega_e; \\ L_\Gamma &= \sum_e \int_{\Omega_e} \frac{\rho c}{\Delta t}{}^{n-1}T_{(M)} P_M \Omega_\Gamma^M \, d\Omega_e H_\Gamma = \sum_e \int_{\partial\Omega_{he}} \Omega_\Gamma^M P_M q_p \, d\partial\Omega_{he}; \\ K_\Gamma &= \sum_e \int_{\partial\Omega_{ce}} \Omega_\Gamma^M P_M h_c T_a \, d\partial\Omega_{ce} \end{aligned} \tag{7}$$

The finite-element equation of the present elastostatic approach is given by [3]

$$\times \begin{bmatrix} \mathbf{A}_{vv} & -\mathbf{D}_{vv} \\ -\mathbf{D}_{vv}^T & \mathbf{0} \end{bmatrix} \begin{bmatrix} \mathbf{t}_v \\ \mathbf{u}_v \end{bmatrix} = \begin{bmatrix} -\mathbf{A}_{vp} & \mathbf{D}_{vp} \\ \mathbf{D}_{pv}^T & \mathbf{0} \end{bmatrix} \begin{bmatrix} \mathbf{t}_p^M + \mathbf{t}_p^T \\ \mathbf{u}_p \end{bmatrix} - \begin{bmatrix} 0 \\ \mathbf{f}_p + \mathbf{p}_p \end{bmatrix}, \tag{8}$$

where submatrices of the system matrices are given by

$$\begin{aligned} A_{\Lambda u v \Gamma s t} &= \sum_e \int_{\Omega_i} \Omega_\Lambda^N S_N g_{(\Lambda)u}^a g_{(\Lambda)v}^b A_{abcd} g_{(\Gamma)s}^c g_{(\Gamma)t}^d T_L \Omega_\Gamma^L \, d\Omega \\ D_{\Lambda u v}^{\Gamma q} &= \sum_e \int_{\Omega_\blacklozenge} \Omega_\Lambda^N S_N U_a^K \Omega_K^\Gamma g_{(\Lambda)u}^a g_{(\Lambda)v}^{(\Gamma)q} \, d\Omega \\ f^{\Lambda q} &= \sum_e \int_{\Omega_\blacklozenge} g_a^{(\Lambda)q} \Omega_M^\Lambda V^M f^a \, d\Omega \\ p^{\Lambda q} &= \sum_e \int_{\partial\Omega_{it}} g_a^{(\Lambda)q} \Omega_M^\Lambda V^M p^a \, d\partial\Omega \end{aligned} \tag{9}$$

The above expressions should be evaluated for each free degree of freedom (dof) connected to the pair of global nodes Λ and/or Γ of the finite-element mesh, where Ω_Λ^L is the connectivity operator, which maps the set of global nodes Λ into the set of local nodes N defined on each element, and vice versa.

In (7) T^L and $\boldsymbol{q}^L$ are nodal values of the temperature scalar T and flux vector $\boldsymbol{q}$ at local node L, respectively. Further, P_L and V_L are corresponding values of the interpolation functions at local node L, while $P_{L,a}$ is its derivative in connective coordinates of an element. More, ρ is the density, k_{ab}^{-1} the inverse of the second order conductivity tensor in connective coordinates of an element, c the specific heat, h_c the convection coefficient, q_p is prescribed heat flux, s the heat source in the volume of an finite element, T_a the ambient temperature, Δt is increment of time, and ${}^{n-1}T_{(M)}$ the temperature at node M in the previous time increment $n-1$.

In (9) **A** is an operator connecting the fourth order compliance tensor with the stress tensor, which is essentially the expression for the *complementary work* done by the system. Finite element base interpolation functions for approximations of displacement and stress fields at local node L are denoted by S_L and T_L. Further, f^a and p^a are the body forces and boundary tractions in natural coordinates of an element, respectively.

Please cite this article as: D. Mijuca, On a new 3D primal-mixed finite element approach for thermal stress analysis of multi-layered geometrically multiscale structures, Finite Elem. Anal. Des. (2009), doi:10.1016/j.finel.2009.11.001

The transformations of the considered tensorial quantity in that global node, from the coordinate system in nodes (x^i or y^i) to natural local coordinate systems (ξ^a) is done by the use of the Euclidian shifters ($g^a_{(A)u}$). All entries in (7) and (9) are presently calculated by using a $3\times3\times3$ Gaussian integration formula.

The system matrices in (6) and (8) are indefinite, sparse and symmetric. The sparsity comes from intrinsic properties of finite-element approximation functions which have local support only. The storage requirements can be reduced by storing only the upper triangle of the matrix because it is symmetric. It is further reduced by storing only the nonzero entries. The pattern of the matrix and the number of entries are direct functions of the type of finite elements used for the mesh discretization of the model problem and the FE node ordering routine. Elements with more nodes per finite element give rise to denser matrices. The optimal solution of the above system of linear equations, where criteria for optimality are robustness, accuracy and execution time, is investigated in detail in [13].

2.3. Finite element configurations

The different finite-element configurations for transient heat [11] and elasticity [10] analyses are shown in Fig. 1. Each element contains 8 or 20 local nodes for the approximation of primal variable and from 9 to 27 nodes for the approximation of dual variable. The finite-element subspaces for the approximation of the dual variable are usually enriched by additional hierarchical shape functions in order to increase stability. Let us recall that primal variables are temperature and displacement, and that dual variables are heat flux and stress.

The convergence of the finite-element procedure is governed by the solvability and stability of the finite-element configurations used [3]. If some finite element procedure satisfies completeness and compatibility criterions and stability conditions [3,8], it is said that it is *reliable* [5]. It was shown in [10] and [11] that present finite element HC8/27 is reliable up to aspect ratio of 3 orders of magnitude. In the present paper it will be numerically proven that it is reliable for aspect ratio of finite elements up to 6 order of magnitude and scale resolution of the model problem up to 7 orders of magnitude, even if the mesh is highly distorted or material is incompressible. That makes the present finite element suitable with bridging the scales with simulation approaches on particle levels [14].

2.4. System matrix

The system matrices in (6) and (8) are sparse, symmetric and indefinite [8]. The indefiniteness of system matrix impose the crucial difficulty in solving saddle-point problem like this, which posses both positive and negative eigenvalues. In addition, present system matrices are far from being banded, so some classical solution procedures, direct methods such as Cholesky decomposition or iterative methods like conjugate gradients, cannot be applied directly [3]. The remedy is to perform an additional reordering to limit the amount of fill-in and operations.

Leading concepts in the development of efficient solution algorithms is to take advantage of the presence of many zeros, and to store and operate only with *entries* (nonzero system matrix terms). During the elimination process, the crucial requirement is to maintain sparsity in the factors in order to minimize the storage and work required for factorization. It is also important to pay great attention to the numerical stability of the factorization. The direct solver MA57 and matrix scaling routine MC64 [17] are presently used. The MA57 is a sparse symmetric linear solver using a multifrontal approach with a choice of ordering schemes. It solves both positive definite and indefinite systems of equations. Like in most sparse direct solvers, the algorithms are organized in three distinct computational phases: analyze, factorize and solve. The more details on time efficiency of the present approach can be found in [13].

2.5. The mathematical convergence requirements

As the finite element mesh is refined, the solution of discrete problem should approach to the analytical solution of the mathematical model, i.e. to converge. The convergence requirements for shape functions of isoparametric element can be grouped into three categories, that is: completeness, compatibility and stability [3,8]. *Consistency* and *stability* imply convergence. If some finite element approach satisfies *completeness* and *compatibility* criterions, it is said that it is *consistent*.

Completeness criterion requires that elements must have enough approximation power to capture the analytical solution in the limit of a mesh refinement process. That is, the finite element approximation functions must be of a certain polynomial order ensuring that all integrals in the corresponding weak formulation are finite. Specifically, if m is variational index calculated as the highest spatial derivative order that appears in the energy functional of the relevant boundary value problem, than the element base approximation functions must represent exactly all polynomial terms in order $\leq m$ in finite element coordinate system. A set of shape functions that satisfies this condition is called m-complete.

Further, *compatibility* criterion requires that finite element shape functions should provide displacement continuity between elements (to prevent artificial material gaps during the deformation). Consequently, trial functions must be C^{m-1} continuous between interconnected elements, and C^m piecewise differentiable inside each element.

In the present finite element approaches, given by (1) and (3), all variable fields have variational indices $m=1$. On the other hand, test and trial approximation functions are taken from the continuous spaces (H^1, H^{1n} or $H^{1n\times n}$), the space of all vector fields that are square integrable and have square integrable gradients.

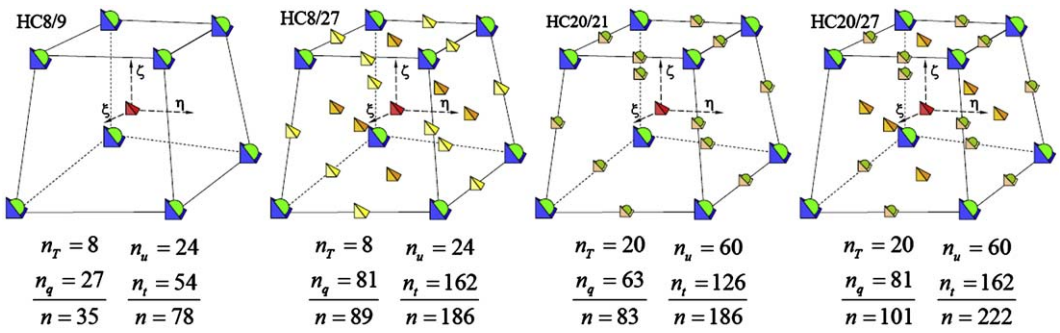

Fig. 1. The primal-mixed finite element family HC.

Please cite this article as: D. Mijuca, On a new 3D primal-mixed finite element approach for thermal stress analysis of multi-layered geometrically multiscale structures, Finite Elem. Anal. Des. (2009), doi:10.1016/j.finel.2009.11.001

Therefore, all integrals in the corresponding weak formulations (1) and (3) are finite. Consequently, the completeness and compatibility requirements are satisfied for both presently considered physical problems. Accordingly, present finite element approaches are *consistent*.

Further, if the stability conditions are satisfied, there will be no non-physical zero-energy modes (kinematic modes). Therefore, the low order test which checks for the zero energy modes, so-called sufficient conditions for solvability (or Eigenvalue analysis) is satisfied if the finite element is stable (see [10] for further details). In Hellinger–Reissner's principles, it is provided if two necessary conditions for stability, are satisfied. The first stability condition is represented by the ellipticity on the kernel condition. The second stability condition is represented by the so-called inf-sup condition (LBB condition) [18]. The analytical verification of these conditions can be difficult [3].

Many mixed finite elements known in the literature utilize the fact that the dual variable is required to have square integrable divergence, but the entire gradient need not exist. That is, the dual variable is sought in H^{div} not in the smaller space H^1. Nevertheless, it introduces the artificial discontinuity of dual variable (e.g. stress) in the absence of the material discontinuity.

However, the satisfaction of the inf-sup condition ensures solvability and optimality of the finite element solution. There are only several finite elements which satisfies this condition in the known literature [18]. More, it is dependent of the number of finite elements in the mesh (mesh size).

It is shown in [10,11] that present FE satisfies all these criteria in geometrically non-multiscale analysis, for both, regular and extremely distorted finite element meshes, and for compressible and nearly incompressible materials. The first stability condition is *a priori* satisfied for present FE formulation, and it is also mesh size undependable.

If some finite element procedure is *consistent* and satisfies *stability* conditions [3,8], it is said that it is *reliable*. In particular, finite element is reliable if the accuracy of the finite element solution does not drastically decrease when some geometric or material properties are changed in the mathematical model for a given finite element mesh [5].

Therefore, because present approaches satisfy first stability condition regardless of the mesh size, we have to prove second stability condition, only. The second stability condition is satisfied if value γ_h, following from LBB (Ladyzhenskaya, Babuška, Brezzi) condition (see [19], p. 76, Eq. (3.22)) remains bounded above zero for the meshes of increasing density. Nevertheless, verification of this condition involves an infinite number of meshes, and it cannot be performed analytically. It is, rather, performed numerically [19] for a limited sequence of meshes of increasing refinement. Consequently, numerical inf-sup test is represented by generalized eigenvalue problem, in matrix notation given by

$$\mathbf{D}_h^T\mathbf{A}^{-1}\mathbf{D}_h\boldsymbol{x} = \lambda\mathbf{C}_h\boldsymbol{x} \tag{10}$$

where **D** and **A** are matrix entries in (8). And matrix **C** is the stiffness matrix from the corresponding displacement based (primal) finite element method (see [10]). If the inf-sup values, for chosen sequence of finite element meshes, do not show decrease toward zero (meaning that the $\gamma = \sqrt{\lambda_{\min}}$ values stabilize at some positive level) it can be said that inf-sup test is passed. The results of the inf-sup test for the present finite element configuration HC8/27 are given in Section 3.1.

3. Numerical examples

Several model problems from thermo-mechanics with geometrical *scale resolution* up to 8 orders of magnitude, and *aspect ratio* up to 7 orders of magnitude, are presently investigated (for terminology see Section 1). They are used to test reliability, time efficiency and accuracy of the present primal-mixed finite element approach HC8/27. The performance with respect to scaling is highlighted. Model problems with high aspect ratio investigated in Examples 3.1, 3.3, 3.4 and 3.5. Highly distorted hexahedral finite elements, where hexahedra is degenerated to tetrahedron or *L* like shape, are considered in Examples 3.1 and 3.2. Multimaterial model problems, as bimetallic strip and thermally coated shaft, are analyzed in Examples 3.4 and 3.5. The inf-sup test on multiscale regular, highly distorted, compressible and incompressible unit brick, is performed in Example 3.1.

The results are, where appropriate, compared with primal hexahedral finite element H8 and analytical solutions [20]. Finite element H8 is based on the primal finite element approach, namely, *displacement finite element method* with incompatible displacement modes (so-called bubble modes) introduced into the element [21], which are eventually eliminated from the element stiffness matrix by the static condensation procedure. A special integration scheme is used to ensure that H8 passes the patch test, while stress field is obtained *a posteriori* and smoothed by the local stress averaging.

The execution time efficiency of the present approach is elaborated in Section 3.4.

3.1. Inf-sup test in multiscale analysis

The inf-sup test (second stability condition) of the present finite element HC8/27 in the geometrically multiscale analysis is performed on the unit brick model problem, for regular and extremely distorted finite element meshes. The aspect ratio of finite elements goes up to 6, while scale resolution of model problem goes up to 7 orders of magnitude. The two cases of materials are considered. The two model problems, of compressible ($\nu = 0.3$) and nearly incompressible ($\nu = 0.49$) materials, are investigated. The Young's modulus is E=1.

Several model problems of increasing refinement are considered. The mesh pattern along x, y and z axes is taken to be $2N \times 2 \times 2$, for $N = 1, 2, 3, 4, 6$. Accordingly, the first model problem has two elements layers per x axis, which have length of 0.999999 and 0.000001, respectively. Therefore, in undistorted mesh for the N=6, the minimal axial dimension of FE is $h_{\min} = 1.66 \times 10^{-7}$. The maximal axial dimension of the FE for all problems is $h_{\max} = 0.5$, so the maximal aspect ratio is $h_{\max}/h_{\min} = 3 \times 10^6$ (i.e. 6 order of magnitude), while scale resolution is $1/h_{\min} = 1.66 \times 10^7$ (i.e. 7 orders of magnitude).

For extremely distorted meshes, the midside points are moved from $M(x, 0.5.0.5)$ positions, to $M(x, 0.7.0.7)$, and maximal aspect ratio is even higher: $h_{\max}/h_{\min} = 4.4 \times 10^6$, while maximal internal angle is 157°, as shown in Fig. 2.

Three model problem cases are reported. The first case is for compressible material and regular mesh, the second case is for compressible material and extremely distorted mesh, and the third case is for nearly incompressible material and extremely distorted mesh. The results are plotted in Fig. 2, from right to left for meshes of increasing refinement, in the form $\log(\gamma_{\min}) = f(1/N)$, where $\gamma_{\min} = \sqrt{\lambda_{\min}}$ is the square root of minimal eigenvalue, see (14).

We can see from Fig. 2, that inf-sup curves of finite element HC8/27 do not show decrease toward zero regardless of aspect ratio and mesh pattern N. They remain stabilized at some level. Therefore, we may conclude that finite element HC8/27 passes present inf-sup test for compressible and nearly incompressible materials, regardless of level of mesh distortion, for aspect ratio up to 4.4×10^6 (5 orders of magnitude). It should be noted that

Please cite this article as: D. Mijuca, On a new 3D primal-mixed finite element approach for thermal stress analysis of multi-layered geometrically multiscale structures, Finite Elem. Anal. Des. (2009), doi:10.1016/j.finel.2009.11.001

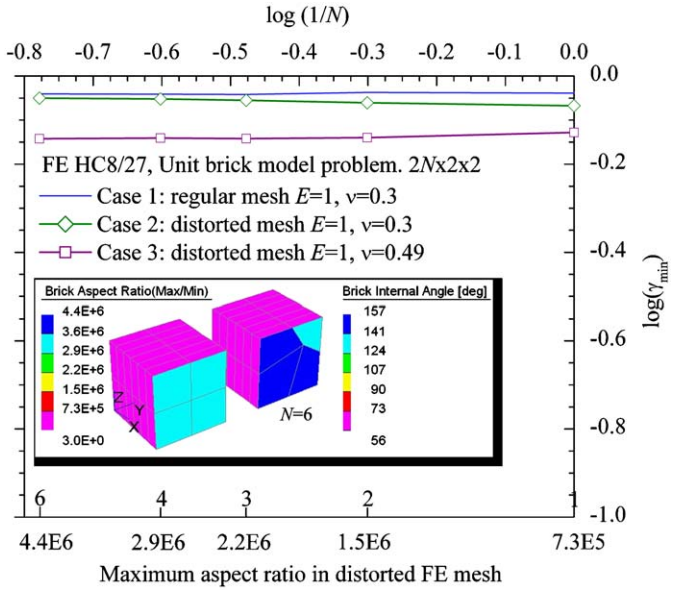

Fig. 2. Unit brick. Inf-sup stability test per multiscale aspect ratio.

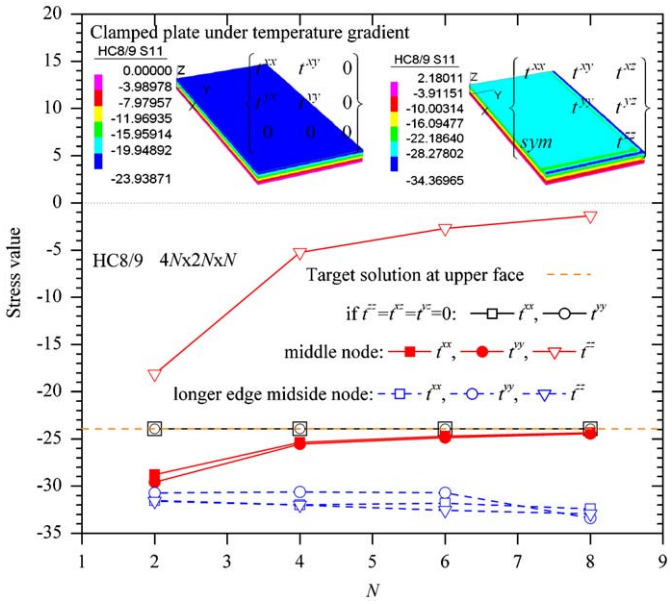

Fig. 3. Clamped plate. Stress convergence.

inf-sup test FE HC8/27 tests for the other model problems, with different geometry, are satisfied also, and will be reported in the next paper.

Keeping in mind that it is already proven in [10] that present finite element passes first stability condition (which *a priori* satisfied), and that it satisfy *completeness* criterion and *compatibility* criterion, we may say that present finite element is reliable under definition set in Section 1.

3.2. Clamped plate under sudden temperature change

The motive for the present example is to check if present approach is capable to mimic the analytical solution obtained by plate theory, and also, how the target solution is changed if there is no simplification imposed on stress tensor components.

The clamped isotropic rectangular plate with dimensions $8\times4\times0.25\,[\mathrm{m}]$ at reference temperature $T_R=294.15\,\mathrm{K}$, is presently investigated. Its upper side is suddenly exposed to the temperature $T=350\,\mathrm{K}\Omega$, thus $\partial T/\partial z=55.85\,\mathrm{K}$. The plate is made from concrete with compressive strength $fc=40\,\mathrm{MPa}$. Young's modulus $E=34290\,\mathrm{MPa}$, and Poisson's ratio $\nu=0.2$. The coefficient of thermal expansion $\alpha=0.00001^{\circ}/\mathrm{K}$.

Unconstrained plate would normally assume a spherical curvature with radius

$$r=h/(\nabla T\alpha), \tag{11}$$

where h is the distance between the hot and the cold face. Nevertheless, if the edges are fixed, the plate will be held flat by resulting uniform edge moments. The maximum bending stress is

$$t^{xx}=\nabla T\alpha E/(1-\nu), \tag{12}$$

which is obtained by the modified Kirchhoff plate theory ([20], pp. 583, Case 9) by neglecting transversal normal and shear stress components ($t^{zz}=t^{xz}=t^{yz}=0$). In the present case analytical solution is $t^{xx}=-23.93871$.

Four finite element HC8/9 meshes with increasing refinement, where $N=2,4,6,8$, are analyzed. The nodes at the clamped edges have constrained displacements in all directions. In the first case (CASE1) we will assume that $t^{zz}=t^{xz}=t^{yz}=0$. In the second case (CASE2) all 6 components of stresses will be solution variables. It should be emphasized that stresses are singular at the corner

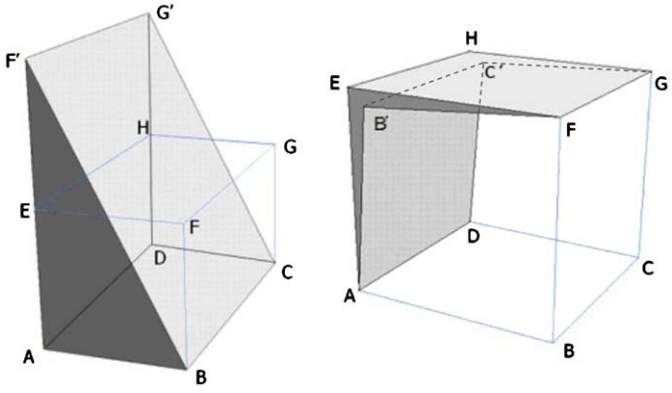

Fig. 4. Highly distorted finite elements.

nodes. Stress results obtained by present HC8/9 approach, at upper midside node and upper midedge node (clamped edge), are shown in Fig. 3, for both full and constrained stress tensor.

We can see from Fig. 4, that in CASE1 the analytical solution is obtained for all considered mesh refinements. In addition, as predicted by plate theory all nodes on the upper face of the model has that same value for both in-plane stress components, t^{xx} and t^{yy}. The stresses on the model down face are zero.

Further, in CASE2 we can see from Fig. 4 that at upper face midside node $M(0,0,0.25)$, stress t^{xx} converges to the slightly greater value than predicted by plate theory. The in-plane normal stress component t^{yy} is of similar value, while transversal normal stress component t^{zz} converges to zero as expected. The transversal shear stress components converge to zero also, as expected. On the other hand, the situation is different for nodes at the clamped edges.

More, the results for the upper face midedge node $C(0,0.2,0.25)$ are shown in Fig. 4, also. We can see that singularity of stress t^{xx} is captured so it has greater value than analytical one.

Therefore, we can see that classical plate theory is not capable of capturing the stress singularity at the clamped edge, but give us an accurate estimate of the stress at the interior points of thin body, only.

Please cite this article as: D. Mijuca, On a new 3D primal-mixed finite element approach for thermal stress analysis of multi-layered geometrically multiscale structures, Finite Elem. Anal. Des. (2009), doi:10.1016/j.finel.2009.11.001

To conclude, present approach can give us analytical plate theory solution if same simplification on stress tensor is assumed. On the other hand, full theory gives us more physically meaningful results, for example, with capturing the maximal stresses on the physical boundaries over the fixed edges, while stress converges to the analytical solution at interior nodes. It is in agreement with singular nature of stresses on clamped edges. Observed inconsistency in results between classical plate theory and present full theory approach, is a good ground for the further experimental measurements. Therefore, we can say that plate theory is just a subset of the present one.

3.3. Clamped beam under sudden temperature change

The quadratic clamped beam is suddenly exposed on upper face, from reference temperature $T_R = 294.15\,\mathrm{K}$ to $T = 350\,\mathrm{K}$. Young's modulus and Poisson's ratio are $E = 34290\,\mathrm{MPa}$ and $\nu = 0.2$, respectively. The coefficient of thermal expansion is $\alpha = 0.00001^{\circ}/\mathrm{K}$. The dimension of the bar is $12 \times 1 \times 1\,[\mathrm{m}]$, in x, y and z axes direction, respectively. The beam is fully fixed on its ends. Resulting uniform edge moments will keep the plate flat. The maximum bending stress is $t^{xx} = \nabla T \alpha E$ [20]. This formula is obtained by modified simple beam theory in which it is assumed that $t^{yy} = t^{zz} = t^{xy} = t^{xz} = t^{yz} = 0$. In our case $t^{xx} = -19.15097\,\mathrm{MPa}$. The sequence of finite element meshes with pattern $12N \times 2N \times 2N$, where $N = 1, 2, 3, 4$, are considered. In this example stress is singular at the physical boundaries of the clamped edges.

The first goal is to test if present fully 3D approach can simulate the simple beam theory, that is, to obtain the analytical solution of the simple beam theory. Second goal is to test the robustness of present approach to high mesh distortion, scale resolution and high aspect ratio of its finite elements. The third goal is to see how the character of stress field is changed when full theory (no simplification on geometry or stress tensor) is used, instead of simplified one.

As in the present example, in the first case (CASE1) we will assume that $t^{zz} = t^{xz} = t^{yz} = 0$. In the second case (CASE2) all 6 components of stresses will be solution variables. Nodes on the clamped edges are fully fixed. The mesh pattern is given by $12N \times 2N \times 2N$, for $N = 1, 2, 3, 4$. Convergence of results per stress component t^{xx} at characteristic nodes, upper corner $C(0\,1\,1)$ and midedge $M(6,1,1)$ nodes, obtained by both considered cases, are presented in Tables 1 and 2.

We can see from Table 1 that for the regular finite element mesh in CASE1 we obtain the analytical solution irrespectively of the mesh parameter N. On the other hand, in the CASE2, the solutions at the midspan node M converge from below to the analytical solution, while at the corner node that is on clamped edge singular value of stress is reported.

Let us now investigate CASE2 for highly distorted and multiscale mesh in yOz planes (cross sections). Upper layer of finite elements will be highly degenerated, as depicted by left and right figures in Fig. 4. The thickness of the upper elements layer will be $1 \times 10^{-6}\,\mathrm{m}$. Consequently, the model problem will look like in Fig. 5.

For highly distorted multiscale mesh the results are given in Table 2. As for the regular mesh, the solutions for t^{xx} at the midspan node M converge from below to the analytical solution, while at the corner node that is on clamped edge singular value of stress is reported.

Comparing the results in Tables 1 and 2, we can notice that present approach is robust to mesh distortion. It was for expected because we prove that present finite element passes inf-sup test in similar model problem geometry (see Section 3.1).

Let us now investigate the distribution of the stress component t^{xx} on the upper edge. One fourth of the model problem is examined due to the symmetry. Finite element mesh $(96+16) \times 1 \times 4$ is considered. In order to diminish the effects of stress singularity on the clamped edge, 16 finite element layers are put over $1\,\mu$m near it. Consequently, the maximal aspect ratio will be almost 7 orders of magnitude. Temperature loading changes through z direction only, so it is enough to have 1 finite element along y direction. The finite element configurations HC8/9 and HC8/27 are considered, without and with simplification on stress tensor. The results are compared with analytical results and

Table 1
Clamped beam under temperature gradient: regular FE HC8/9 mesh.

	Clamped beam loaded by transversal temperature gradient. Regular Mesh $12N \times 2N \times 2N$. FE HC8/9. Analytical solution -19.15097.					
	t^{xx} *at corner node* $C(0,1,1)$			t^{xx} *at midspan node* $M(6,1,1)$		
N	CASE 1	CASE 2	Relative error (%)	CASE 1	CASE 2	Relative error (%)
1	−19.15097	−30.65553	60.07	−19.15097	−20.49503	7.02
2	−19.15097	−36.10571	88.53	−19.15097	−20.08562	4.88
3	−19.15097	−43.16012	125.37	−19.15097	−20.00783	4.47
4	−19.15097	−49.24679	157.15	−19.15097	−19.71298	2.93

Stress t^{xx} convergence.

Table 2
Clamped beam under temperature gradient: highly distorted multiscale FE HC8/9 mesh.

		Clamped beam loaded by temperature gradient. Case 2. Highly distorted multiscale FE HC8/9.mesh, $12N \times 2N \times 2N$. Analytical solution -19.15097.			
		t^{xx} *at corner node* $C(0,1,1)$		t^{xx} *t midspan node* $M(6,1,1)$	
N	Maximal aspect ratio	CASE 2	Relative error (%)	CASE 2	Relative error (%)
2	500000	−34.06640	77.88	−20.86432	8.95
3	333333	−40.18221	109.82	−20.37795	6.41
4	250000	−46.22371	141.36	−20.12185	5.07

Maximal aspect ratio. Stress t^{xx} convergence. Relative error.

Please cite this article as: D. Mijuca, On a new 3D primal-mixed finite element approach for thermal stress analysis of multi-layered geometrically multiscale structures, Finite Elem. Anal. Des. (2009), doi:10.1016/j.finel.2009.11.001

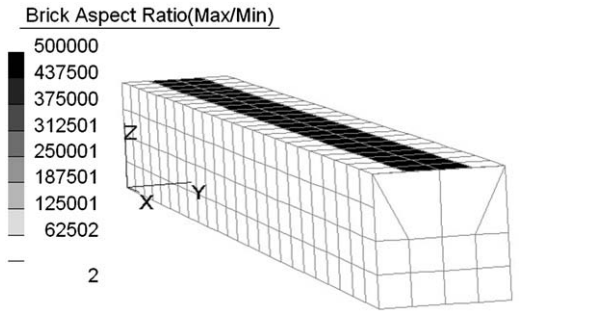

Fig. 5. Clamped beam. Aspect ratio.

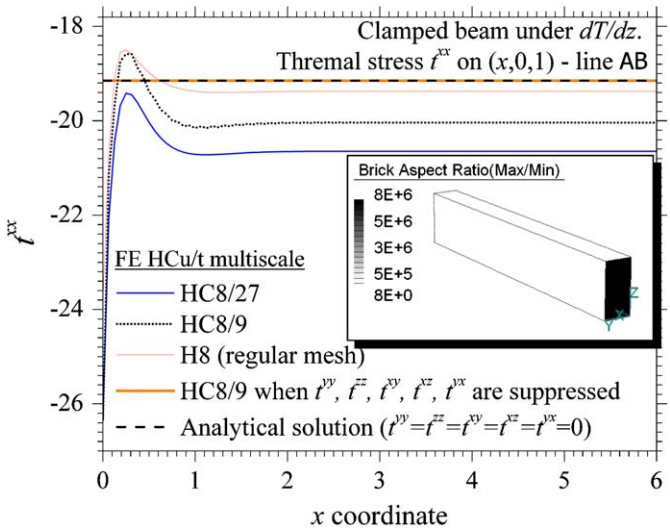

Fig. 6. Clamped beam. Stress distribution over regular mesh.

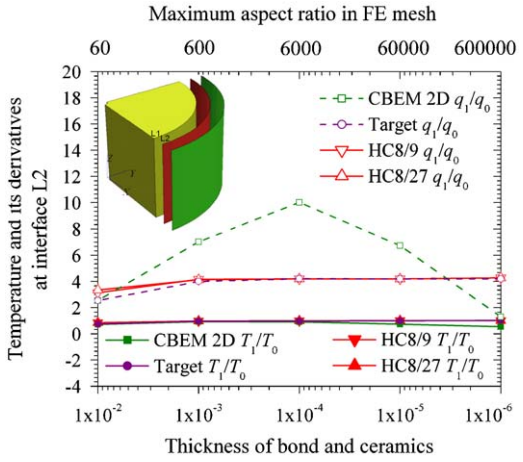

Fig. 7. Coated shaft. Temperature and temperature gradients.

results obtained by finite element H8 based on assumed displacement finite element method with *a posteriori* local stress averaging (primal approach). The aspect ratios of the model problem and results are shown in Fig. 6.

We can see from Fig. 6, that present finite element HC8/9 with neglecting all stress components except t^{xx}, as in beam theory, give us analytical results of the beam theory. Further, finite element HC8/9 with full stress tensor approximation captures the stress singularity with local stress concentration, but afterwards has uniform value slightly about 4.8% greater than analytical. More, finite element HC8/27 has similar character of distribution, but has 7.9% greater stresses at interior points. Primal finite element H8 has similar behaviour but interior stresses 1.8% different from analytical.

Let us emphasize that similar difference in analytical results and experiment, is reported also in [22] (Fig. 9 and 15). It is shown there that difference in measured and analytical results goes up to 17%.

3.4. Long steel coated shaft

The simulation of the coated materials is of particular interest to industry in order to control the level of the interfacial stresses on the surfaces of material discontinuities [23]. Therefore, a hollow shaft covered with microsized coating layer for mechanical and thermal protection, shown in Fig. 7, is presently examined.

The material properties are given in Table 3. The inner and outer radii of the shaft are 0.005 and 0.1 m, respectively. The reference temperature is $T_R = 1273$ K. The prescribed temperatures on inner and outer surfaces are $T_i = 773$ K and $T_o = 1273$ K, respectively.

The coating consists of a bond and ceramic layers of the equal size. In order to test the robustness of present finite element to high distortion, the thickness of the coating (bond and ceramic) is gradually decreased from $h = 10^{-2}$ m to $h = 10^{-6}$ m. Consequently, all stress tensor components, except radial, will be discontinuous on material interfaces and will differ significantly from each other due to the large difference in physical properties of the bonded materials.

The analytical solution is obtained by modified plane strain plate theory [23]. It is presently assumed that height off the shaft is 0.1 m. We will investigate the convergence of the temperature and radial stress component on the interface L2, between bond and ceramics. The temperature distribution is calculated by present finite element thermal approach (6), after which thermal stresses are calculated by (8) without *consistency* error [15] (see Section 2.1).

The sequence of five model problems with decreasing coating thickness $h = 10^{-N}$, where $N = 2, 3, 4, 5, 6$, are analyzed. Model problem is plain strain, so it is enough to set only one finite-element layer along height. One-quarter of the model problem is analyzed due to the symmetry. Bond and ceramic are discretized by 3 layers of finite elements along the radius in all meshes. Consequently, maximum finite element aspect ratio of 600 000 will be in the model problem with coating thickness $h = 10^{-6}$ m.

The results obtained by present finite element HC8/9 and classical plane boundary element method (CBEM) [22] per temperature and stress at interface L2, are shown in Figs. 7 and 8 respectively.

We may see that approach CBEM exhibits spurious oscillation of results. On the other side, present approach is invariant to the size of the coating thickness.

Let us now investigate the distribution of stress components t^{xx}, t^{yy}, t^{zz} and t^{xz} in the radial direction (over x-coordinate) in the region over the surfaces of material discontinuities, L1 and L2. The model problem with thickness of the coating $h = 10^{-6}$ m, is examined. The results are shown in Fig. 9. It can be seen that there are no spurious oscillations of stresses near the material discontinuities.

Let us now briefly analyze the time efficiency of the present approach (see Section 2.4). The more details can be found in [13]. The execution time for three distinct phases in the solution

Please cite this article as: D. Mijuca, On a new 3D primal-mixed finite element approach for thermal stress analysis of multi-layered geometrically multiscale structures, Finite Elem. Anal. Des. (2009), doi:10.1016/j.finel.2009.11.001

Table 3
Long steel coated shaft.

	Long steel coated shaft-material properties				
	Modulus $E \times 10^4$ [MPa]	Poisson's ratio ν	Thermal expansion coefficient $\alpha \times 10^{-5}$[°/C]	Density $\rho \times 10^3$ [kg]	Thermal conductivity k[W/m²C]
Ceramic	1.0	0.25	1.0	4.0	1
Bond	13.7	0.27	1.51	4.0	25
Steel	21.0	0.30	2.0	7.98	25

Material properties.

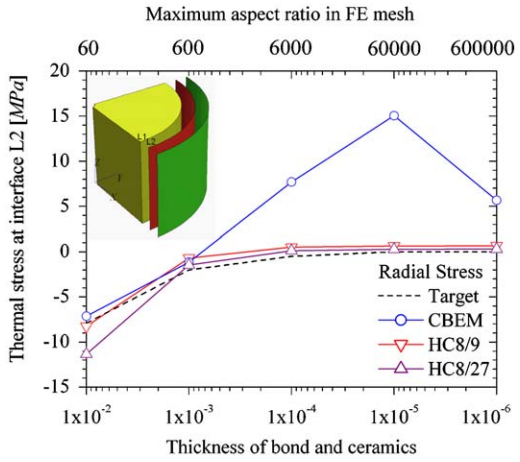

Fig. 8. Coated shaft. Thermal stress at interface.

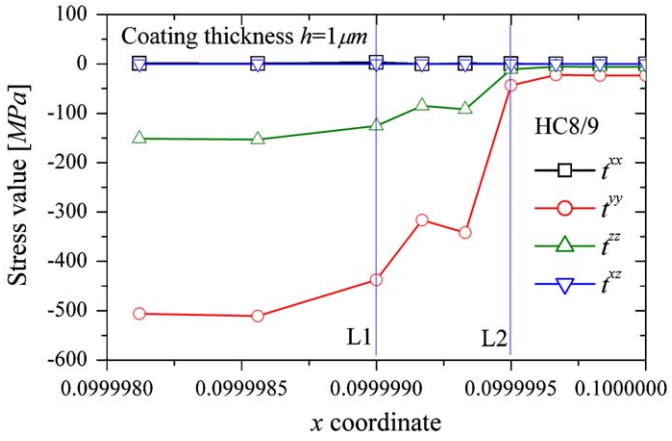

Fig. 9. Coated shaft. Distribution of stress over interfaces.

process, storage requirements and backward error for in-house direct Gaussian solver and MA57 solver with scaling routine MC64, are reported in Table 4. Numerical experiments were conducted on a PC Pentium(R) D CPU 2.8 GHz with 3.25 GB of RAM with Physical Address Extension running under the operating system Microsoft Windows XP Professional Version 2002 Service Pack 2, double precision (64-bit) reals were used, CPU times are given in seconds.

We can see from results reported in Table 5 that scaling the system matrix prior to the factorization using MC64scaling routines considerably improves the execution time. In addition, the storage requirements and number of operations are far smaller. MA57 without scaling was not able to solve some model problems, because the factorization fails due to insufficient storage. Therefore, the conclusion is that scaling generally decreases the storage requirements, decrease the solution time, and enables the solution of systems with much more degrees of freedom. As an interesting aside to this set of problems, the given matrix has many entries of very small size (around 10^{-20}). However, these are significant numbers inasmuch if they are treated as zero, it is not possible to solve the resulting systems because the matrix is singular.

3.5. Bimetallic strip

The motive for present example is to investigate how physical singularity of stresses on the clamped edge and material interface influence the behavior of the present approach using finite elements HC8/9, HC8/27 and HC20/21. The results are compared with results obtained by finite elements H8 and H20 based on assumed displacement based (*primal*) approach where stresses are calculated *a posteriori*. It should be noted that these *primal* finite elements are not designed to be used in spatially multiscale situations because of the hourglass locking [3]. Nevertheless, it will help to emphasize the robustness of present approach.

Bimetallic strips are made of two materials having different coefficients of expansion. It causes the strip to change its curvature when subjected to a change in temperature [20]. The cantilever bimetallic strip of length $l = 10$, width $w = 0.1$, and thickness $h = 0.1$, is analyzed. The beam is stress free at $T_R = 70$ and subjected to a uniform temperature $T_0 = 170$. Both materials has modulus of elasticity $E = 3 \times 10^7$ MPa and Poisson's ratio $\nu = 0.3$. The difference is in coefficients of thermal expansion, $\alpha_1 = 1 \times 10^{-5}$ and $\alpha_2 = 2 \times 10^{-5}$, for the upper and lower material, respectively. All components of stresses except transversal will be singular at the material interface. In addition, clamped edges are lines of discontinuity.

We will assume that the beam longitudinal axe coincide with x direction. Nodes on the clamped edge have suppressed displacements. Analytical solutions, obtained by modified simple beam theory (see [20], page 114) is $t^{xx} = -7500$, for the top surface, and maximal deflection is $u_z = 0.75$. Only one half of the model problem will be analyzed due to the symmetry.

In order to localize the stress singularity on the material interface, we will place very thin layer of finite elements on the both side of the material interface, that is, one layer on each side, with thickness $h_b = 0.0001$ m. Further, we will localize effect of stress singularity on the clamped edge by placing $1/N$ microsized finite elements near the clamped edge with thickness $h_c = 0.000001\,\mathrm{m}/N$. Therefore, the mesh pattern is given by $(10N+N) \times 1 \times (2+1+1+2)$, where $N = 2, 4, 8, 16$.

Consequently, maximal *scale resolution*, that is, ratio of maximal axial dimension of the model problem ($l_{\max}^{\text{model}} = 10$) and minimal axial dimension of finite elements ($h_{\min}^{\text{FE}} = 0.000001/\ 16 = 6.25 \times 10^{-8}$),

Please cite this article as: D. Mijuca, On a new 3D primal-mixed finite element approach for thermal stress analysis of multi-layered geometrically multiscale structures, Finite Elem. Anal. Des. (2009), doi:10.1016/j.finel.2009.11.001

Table 4
Coated cylindrical shaft.

	Coated cylindrical shaft-execution time and storage requirements							
	FE	N	NE	Time				Backward error
				Analyze	Factorize	Solve	Total	
in-house	HC8/9	5776		14.31	0.75	15.06		
	HC20/21	16500		1810.17	4.89	1815.06		
MA57+MC64	HC8/9	5776	280056	0.03	0.50	0.01	0.54	0.8E−12
	HC20/21	16500	1829790	0.17	12.28	0.05	12.50	0.1E−10
	HC8/27	18634	1961070	0.19	4.05	0.06	4.30	0.2E−10
	HC20/27	22122	2785700	0.27	11.59	0.08	11.94	0.3E−10

Execution time and storage requirements.

Table 5
Cantilever bimetallic strip.

	Convergence of maximal displacement u^z Mesh pattern $(10N+N)\times 1\times 4$ for $N=2,4,8,16$ Thickness of the bond layers $h_b=0.0001$ m Thickness of the layers near the clamped edge $h_c=0.000001$ m/N							
N	NEL	Scale resolution $l_{\max}^{\text{model}}/h_{\min}^{\text{FE}}$	Aspect ratio	HC8/9	HC20/21	HC8/27	H8	H20
2	88	2E+07	1E+05	0.6649954	0.7500676	0.5861077	0.7500546	0.7501663
4	176	4E+07	2E+05	0.7311053	0.7500674	0.7131315	0.7500688	0.7499819
8	352	8E+07	4E+05	0.7464689	0.7500664	0.7430614	0.7500615	0.7501227
16	704	2E+08	8E+05	0.7495121	0.7500637	0.7490083	0.7500665	0.7505277
				$u_z=0.75$; $t^{xx}_{\text{target}}=7500$				

Convergence of maximal displacement u^z.

will be $l_{\max}^{\text{model}}/h_{\min}^{\text{FE}}=1.6\times 10^8$ (up to 8 orders of magnitude). Maximal *aspect ratio* of finite elements in the present model problem will be $h_{\max}/h_{\min}=8\times 10^5$, that is almost 6 orders of magnitude.

The convergences of displacements at the beam tip as the mesh is refined for finite elements HC8/9, HC8/27 and HC20/21, are given in Table 5.

It can be seen from Table 5 that tip displacement obtained by finite elements HC8/9, HC8/27 and HC20/21, uniformly converges to the analytical displacement, while *raw* finite elements H8 and H20 oscillates around analytical solution.

Let us now investigate distribution of target stress t^{xx} along the upper edge $(x,0.05,0.05)$. The results for linear finite elements: primal H8 and primal-mixed HC8/27, are shown in Fig. 10.

We can see that present finite element configuration HC8/27 does not exhibit spurious oscillations. Let us recall that this finite element passes inf-sup test (see Example 3.1). It also captures singularity of stress at the clamped edge without oscillation. On the other hand raw finite element H8, based on displacement based finite element method without modification on interpolation functions, exhibits spurious oscillations of the results. Present element is *raw*, also.

Let us now investigate the convergence rate of the present spatially multiscale approach. We will measure the relative displacement error η of the approximated solution u_i^h in accordance to the target solution u_i^{Target}, given by

$$\eta=\frac{|u_i^h-u_i^{\text{Target}}|}{|u_i^{\text{Target}}|} \tag{13}$$

Therefore, the logarithmic relative errors per maximal displacements η vs. logarithm of the number of finite elements *NEL*, are shown in Fig. 11.

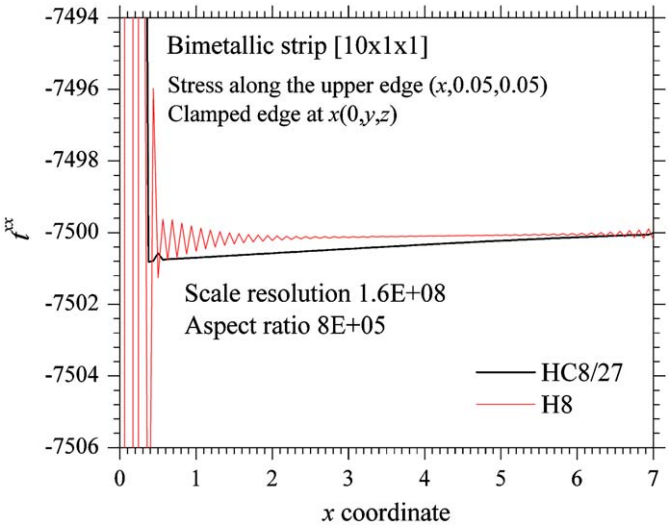

Fig. 10. Bimetallic strip. Distribution of stress.

The convergence results show that finite elements HC8/9 and HC20/27 have quadratic convergence rate in spatially multiscale analysis of model problem loaded by thermal loading.

3.6. Bending dominated case

In order to test the convergence rate of the present approach the model problem in the bending dominated situation [10], a clamped thin quadratic plate loaded by the transverse uniform load $q=-100$, is considered,. The side of a plate is a=2 and

thickness $h=0.01$. Young's modulus is $E=1.7472\times10^7$, and Poisson's ratio $v=0.3$. Only a quarter of the plate is analyzed due to its overall symmetry. The sequence of FE HC8/9 regular $N\times N\times 2$, $N=4,8,16,32,40,48$, and spatially multiscale $N\times N\times 2$, $N=5,10,20,40,50,60$ meshes, are considered. Multiscale mesh is obtained by placing the thin layer of elements, of thickness $h=1\times10^{-4}/\mathrm{N}$, near the clamped edges. In this case, maximal aspect ratio is always 2500. Nevertheless, the scale resolution of the model problem goes up to $1/(8.33\times10^{-6})=1.2\times10^5$ for mesh which has N=60 elements per side. This model has 48×48 interior finite elements of dimension $1-1\times10^{-4}/\ 48\times 1-1\times10^{-4}/48\times0.01/2$, and 12×48 finite elements of dimension $1-1\times10^{-4}/48\times1\times10^{-4}/12\times0.01/2$ per each of clamped edge, and $12\times12'$ corner finite elements $1\times\ 10^{-4}/12\times1\times10^{-4}/12\times0.01/2$. This number of elements should be doubled for second layer of elements per thickness of the plate. Consequently, this model problem has 7200 finite elements in total.

The results for deflection u_z at the center of the plate, based on the plate theory assumptions [20] can be written as

$$u_z=c\frac{qa^4}{D},\quad D=\frac{Eh^3}{12(1-v^2)} \tag{14}$$

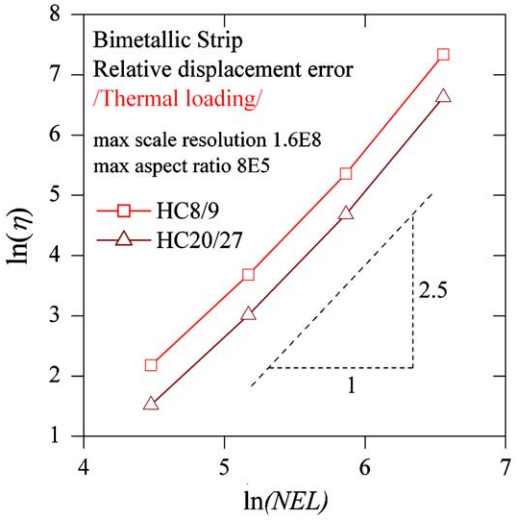

Fig. 11. Bimetallic plate. Relative displacement error.

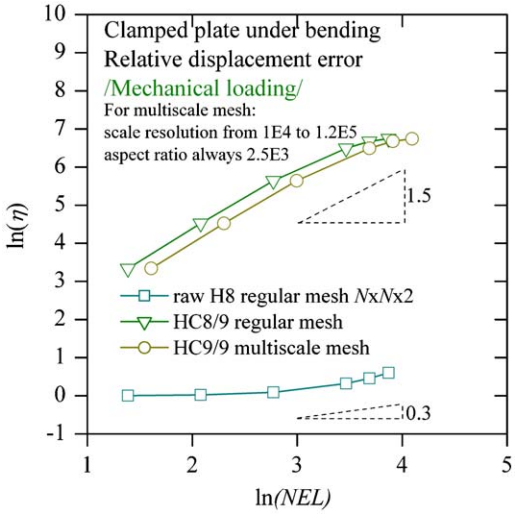

Fig. 12. Clamped plate. Relative displacement error.

where up to 10 digits [24]:

$$c=1.265319087\times10^{-3}. \tag{15}$$

The logarithmic relative errors (13) of the maximal displacements η vs. logarithm of the number of finite elements, for regular and spatially multiscale meshes *NEL*, are shown in Fig. 12.

We can see from Fig. 12, that present finite element HC8/9 approach has almost quadratic convergence rate in regular mesh analysis. In multiscale analysis it has also almost quadratic convergence rate. On the other hand, it can be seen that finite element H8 based on corresponding *raw displacement based* finite element method (primal approach) [3] has convergence rate below 1. The present approach is also *raw* because of it has no any modification on interpolation functions.

4. Conclusion

The reliable and time efficient three-dimensional multifield primal-mixed hexahedral finite element approach in thermoelastic spatially multiscale analysis in multi material solid mechanics, based on Hellinger–Reissner's principle, is presented. The geometrical scale resolutions up to 8 orders of magnitude and aspect ratio of finite elements up to 7 orders of magnitude, are considered. In order to avoid the geometrical invariance error and to enable introduction of displacement and stress constraints in an adequate coordinate systems, the underlying finite element scheme is coordinate independent. It has several essential contributions in accordance to other finite element approaches. Firstly, dual variables, stress and heat flux, are solution variable, also. Secondly, they are also chosen to be from continuous subspaces of finite element functions, allowing physically natural approximation over the discontinuity free regions of the solid body. Thirdly, stress constraints can be introduced as essential boundary conditions. The dimensional reduction theories, as beam and plate, are exactly simulated by suppressing corresponding stress tensor components.

Further, the present approach passes second inf-sup test in spatially multiscale analysis, and it is invariant to high distortion and aspect ratio of finite elements up to 6 orders of magnitude, and scale resolution up to 8 orders of magnitude, for compressible and nearly incompressible materials. Consequently, coated bodies, layered composites or bodies with some inclusions can be efficiently analyzed. Namely, aspect ratio of hexahedral finite elements in the mesh could be up to 6 orders of magnitude, while they are degenerated to tetrahedron and *L* like shapes, without compromising the convergence. In addition, in order to localize singularity, microsized finite elements can be placed adjacent to the surfaces of the material discontinuities. It is shown that by rapid varying of spatial scale over local heterogeneities, the singularity of stress is captured without oscillation. Therefore, present procedure is ideal to be bridged with simulation approaches on particle levels.

More, as stress is solution variable, initial stress and/or strain field is introduced directly, which is used for straightforward coupling of thermal and mechanical analyses without *consistency* error. In addition, nearly incompressible materials are analyzed without volumetric locking, and there are no spurious oscillations of results near singularity.

From the number of benchmark tests performed in thermo mechanically loaded solid bodies, we can see that present approach provides accurate results for an execution time which is at least three orders of magnitude faster than earlier reported results. Further, it is shown that simplified theories, as beam and plate theories, and *primal* finite element approaches, can lead to the substantial underestimation of maximal thermal stresses, which is already noticed in experimental testing. In addition, the

Please cite this article as: D. Mijuca, On a new 3D primal-mixed finite element approach for thermal stress analysis of multi-layered geometrically multiscale structures, Finite Elem. Anal. Des. (2009), doi:10.1016/j.finel.2009.11.001

preliminary results show that it is unconditionally stable in approximation over temporal scales and that it requires much smaller number of time steps than corresponding *primal* approach. The detailed report on approximation over temporal scales will be reported in the next paper.

Acknowledgments

My special thanks go to Iain S. Duff elected Fellow of the Royal Society of Edinburgh, for his collaboration in implementation of solver MA57 and scaling routine MC64 in present approach. The work on present text was supported by the Ministry of Science of Republic of Serbia Grant 144007.

References

[1] Q. Yu, J. Fish, Multiscale asymptotic homogenization for multiphysics problems with multiple spatial and temporal scales: a coupled thermo-viscoelastic example problem, International Journal of Solids and Structures 39 (26) (2002) 6429–6452.
[2] J.I. Özdemir, W.A.M. Brekelmans, M.G.D. Geers, FE^2 computational homogenization for the thermo-mechanical analysis of heterogeneous solids, Computer Methods in Applied Mechanics and Engineering 198 (2008) 602–613.
[3] D.N. Arnold, Mixed finite element methods for elliptic problems, Computer Methods in Applied Mechanics and Engineering 82 (1990) 281–300.
[4] I. Babuska, M. Vogelius, On a dimensional reduction method. III, A-posteriori error estimation and an adaptive approach, Mathematics of Computation 37 (156) (1981) 361–383.
[5] K.J. Bathe, On reliability in the simulation of structural and fluid flow response. Advances in Computational Methods for Simulation, Civil-Comp Press, Edinburgh, 1996, pp. 1–7.
[6] K.S. Chavan, B.P. Lamichhane, B.I. Wohlmuth, Locking-free finite element methods for linear and nonlinear elasticity in 2D and 3D, Computer Methods in Applied Mechanics and Engineering 196 (41) (2007) 4075–4086.
[7] G. Prathap, B.P. Naganarayana, Consistent thermal stress evaluation in finite elements, Computers and Structures 54 (1995) 415–426.
[8] R. Rannacher, F.T. Suttmeier, A feed-back approach to error control in finite element methods: application to linear elasticity, Computational Mechanics 19 (5) (1997) 434–446.
[9] F. Brezzi, M. Fortin, D. Marini, Mixed finite element methods with continuous stresses, Mathematical Models and Methods in Applied Sciences 3 (2) (1993) 275–287.
[10] D. Mijuca, On hexahedral finite element HC8/27 in elasticity, Computational Mechanics 33 (6) (2004) 466–480.
[11] D. Mijuca, A. Ziberna, B. Medjo, A new multifield finite element method in steady state heat analysis, Thermal Science 9 (1) (2005) 111–130.
[12] I.S. Duff, S. Pralet, Strategies for scaling and pivoting for sparse symmetric indefinite problems, SIAM Journal on Matrix Analysis and Applications 27 (2) (2005) 313–340.
[13] I.S. Duff, D. Mijuca, On accurate and time efficient solution of primal-mixed finite element equations in multiscale solid mechanics, Communications in Numerical Methods in Engineering (Article online in advance of print) (2009) doi:10.1002/cnm.1296.
[14] M.S. Shephard, M.A. Nuggehally, B. Franz Dale, C.R. Picu, J. Fish, Component software for multiscale simulation, in: J. Fish (Ed.), Bridging the Scales in Science and Engineering, Oxford University Press, Oxford, 2008.
[15] S. Miranda, F. Ubertini, On the consistency of finite element models, Computer Methods in applied Mechanical Engineering 190 (2001) 2411–2422.
[16] A.A. Cannarozzi, F. Ubertini, A mixed variational method for linear coupled thermoelastic analysis, International Journal of Solids and Structures 38 (2001) 717–739.
[17] M. Arioli, J.W. Demmel, I.S. Duff, Solving sparse linear systems with sparse backward error, SIAM Journal on Matrix Analysis and Applications 10 (2) (1989) 165–190.
[18] K.J. Bathe, The inf-sup condition and its evaluation for mixed finite element methods, Computers and Structures 79 (2001) 243–252.
[19] F. Brezzi, M. Fortin, Mixed and Hybrid Finite Element Methods, Springer, New York, 1991.
[20] R.J. Roark, W.C. Young, Formulas for Stress and strain, fifth ed., McGraw-Hill, New York, 1975.
[21] E.L. Wilson, A. Ibrahimbegovic, Use of incompatible displacement modes for the calculation of element stiffnesses or stresses, Finite Elements in Analysis and Design 7 (1990) 229–241.
[22] A.Y. Elghazouli, B.A. Izzuddin, A.J. Richardson, Composite beams in large buildings under fire—numerical modelling and structural behaviour, Fire Safety Journal 35 (3) (2000) 165–188.
[23] S. Lu, M. Dong, An advanced BEM for thermal and stress analyses of components with thermal barrier coating, Electronic Journal of Boundary Elements 1 (2) (2003) 302–315.
[24] R.L. Taylor, S. Govindjee, Solution of clamped rectangular plate problems, Communications in Numerical Methods in Engineering 20 (10) (2004) 757–765.

Please cite this article as: D. Mijuca, On a new 3D primal-mixed finite element approach for thermal stress analysis of multi-layered geometrically multiscale structures, Finite Elem. Anal. Des. (2009), doi:10.1016/j.finel.2009.11.001